Coupled Systems Mechanics, *Vol. 13, No. 3 (2024) 201-217*
https://doi.org/10.12989/csm.2024.13.3.201

Minimum area for circular isolated footings with eccentric column taking into account that the surface in contact with the ground works partially in compression

Inocencio Luévanos-Soto[1a], Arnulfo Luévanos-Rojas[*2], Victor Manuel Moreno-Landeros[2b] and Griselda Santiago-Hurtado[3c]

[1]Instituto de Investigaciones Multidisciplinaria, Universidad Autónoma de Coahuila, Blvd. Revolución No, 151 Ote, CP 27000, Torreón, Coahuila, México
[2]Facultad de Ingeniería, Ciencias y Arquitectura, Universidad Juárez del Estado de Durango, Av. Universidad S/N, Fracc. Filadelfia, CP 35010, Gómez Palacio, Durango, México
[3]Facultad de Ingeniería Civil, Universidad Autónoma de Coahuila, CP 27276, Torreón, Coahuila, México

(Received February 24, 2024, Revised March 15, 2024, Accepted March 15, 2024)

Abstract. This study aims to develop a new model to obtain the minimum area in circular isolated footings with eccentric column taking into account that the surface in contact with the ground works partially in compression, i.e., a part of the contact area of the footing is subject to compression and the other there is no pressure (pressure zero). The new model is formulated from a mathematical approach based on a minimum area, and it is developed by integration to obtain the axial load "P", moment around the X axis "M_x" and moment around the Y axis "M_y" in function of σ_{max} (available allowable soil pressure) R (radius of the circular footing), α (angle of inclination where the resultant moment appears), y_0 (distance from the center of the footing to the neutral axis measured on the axis where the resultant moment appears). The normal practice in structural engineering is to use the trial and error procedure to obtain the radius and area of the circular footing, and other engineers determine the radius and area of circular footing under biaxial bending supported on elastic soils, but considering a concentric column and the contact area with the ground works completely in compression. Three numerical problems are given to determine the lowest area for circular footings under biaxial bending. Example 1: Column concentric. Example 2: Column eccentric in the direction of the X axis to 1.50 m. Example 3: Column eccentric in the direction of the X axis to 1.50 m and in the direction of the Y axis to 1.50 m. The new model shows a great saving compared to the current model of 44.27% in Example 1, 50.90% in Example 2, 65.04% in Example 3. In this way, the new minimum area model for circular footings will be of great help to engineers when the column is located on the center or edge of the footing.

Keywords: axial load; circular isolated footings; minimum area; moment around the X axis; moment around the Y axis; surface in contact with the ground works partially in compression

---

*Corresponding author, Ph.D., E-mail: arnulfol_2007@hotmail.com
[a]Ph.D. Candidate, E-mail: inocencio.luevanos@ujed.mx
[b]Ph.D., E-mail: victor_moreno_landeros@uadec.edu.mx
[c]Ph.D., E-mail: santiagog@uadec.edu.mx

http://www.techno-press.org/?journal=csm&subpage=8 ISSN: 2234-2184 (Print), 2234-2192 (Online)

1. Introduction

The main element of a building is the foundation and its essential function is the transmission of loads supported by the structure to the subsoil.

The reinforced concrete foundations can be classified according to their function as: isolated footings that support a column and can be circular, square and rectangular in shape, combined footings that support two or more columns and can be rectangular, trapezoidal, strap, L (Corner) and T in shape, strap footings are two or more isolated footings joined by a beam, raft or mat foundation that support an entire building and can be circular, square, rectangular, trapezoidal, L (Corner) and T in shape.

The main contributions on the bearing capacity of the soil, soil-structure interaction, experimental tests for footings and settlement behavior in foundations under biaxial bending have been presented by several researchers (Ramu and Madhav 2010, Lee *et al.* 2015, Kaur and Kumar 2016, Dagdeviren 2016, Hadzalic *et al.* 2018a, b, c, 2020, Turedi *et al.* 2019, Golewski 2019, Luat *et al.* 2020, Ibrahimbegovic *et al.* 2021).

The strong interest in foundation design has been stimulated by the quick development of the mathematical models in the recent decades. The mathematical models for the design or contact area with the ground have been presented for isolated footings under biaxial bending assuming that the contact area of the footing with the soil works entirely under compression (Agrawal and Hora 2012, Al-Ansari 2013, 2014, Alijani and Bidgoli 2018, Alazwari *et al.* 2021, Anil *et al.* 2017, Basudhar *et al.* 2012, Gör 2022, Himeur *et al.* 2022, Jelusic and Zlender 2018, Khajehzadeh *et al.* 2014, 2017a, Lezgy-Nazargah *et al.* 2022, Malapur *et al*, 2018, Luévanos-Rojas 2014a, b, 2015a, 2016a, 2023a, Rad 2012, Rawat and Mittal 2018, López-Chavarría *et al.* 2017a, b, 2019). The mathematical models for the design or contact area with the ground have been developed for combined footings under biaxial bending in each column assuming that the contact area of the footing with the soil works entirely under compression (Luévanos-Rojas 2015b, 2016b, 2023b, Mohebkhah 2017, Luévanos-Rojas *et al.* 2017b, 2018a, b, 2020, Rizwan *et al.* 2012, Velázquez-Santillán *et al.* 2018, Aguilera-Mancilla *et al.* 2019, Yáñez-Palafox *et al.* 2019, Pasillas-Orona *et al.* 2020, García-Galván *et al.* 2022a, b, Rivera-Mendoza *et al.* 2022, Garay-Gallegos *et al.* 2022, Moreno-Hernández *et al.* 2022, Garcia-Graciano *et al.* 2022). The mathematical models for the contact area with the ground have been investigated for some footings under biaxial bending assuming that the contact area of the footing with the soil works partiality under compression as: circular isolated footings (Soto-García *et al.* 2022), rectangular isolated footings (Vela-Moreno *et al.* 2022) and rectangular combined footings (Montes-Páramo *et al.* 2023). The mathematical models for the complete design for some footings under biaxial bending assuming that the contact area of the footing with the soil works partiality under compression as: circular isolated footings (Kim-Sanchez *et al.* 2022), rectangular isolated footings (Luévanos-Rojas 2023c).

The current documents closest to the topic addressed here are: The current papers on isolated footings that show the minimum contact area with the ground that work partially in compression for circular isolated footings (Soto-García *et al.* 2022) and rectangular isolated footings (Vela-Moreno *et al.* 2022), these works are presented only for columns located in the center of the footing. The current study with eccentric column that shows the minimum cost design for rectangular isolated footings proposed by Luévanos-Rojas (2023a), but this work presents the area in contact with the ground working completely under compression.

This paper presents a new model to obtain the minimum area for circular isolated footings with eccentric column taking into account that the surface in contact with the ground works partially in

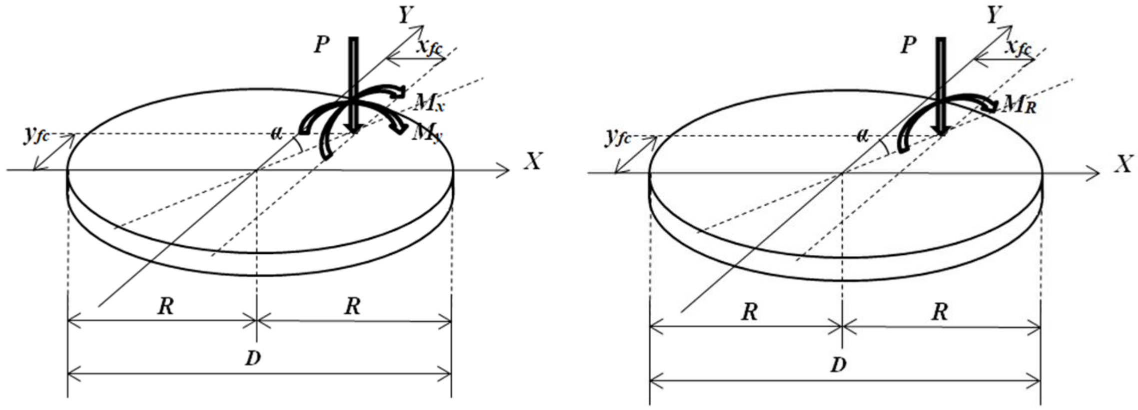

(a) Load and real moments "P", "M_x" and "M_y" (b) Load and resultant moments "P" and "M_{RT}"

Fig. 1 Circular isolated footing with an eccentric column

compression, i.e., a part of the contact area of the footing is subject to compression and the other there is no pressure (pressure zero). The methodology is developed by integration to obtain the axial load "P", moment around the X axis "M_x" and moment around the Y axis "M_y" in function of σ_{max} (available allowable soil pressure) R (radius of the circular footing), α (angle of inclination with respect to the Y axis where the resultant moment appears), y_0 (distance from the center of the footing to the neutral axis measured on the axis where the resultant moment appears). Three numerical problems are given to determine the lowest area for circular footings under biaxial bending. Example 1: Column concentric. Example 2: Column eccentric in the direction of the X axis to 1.50 m. Example 3: Column eccentric in the direction of the X axis to 1.50 m and in the direction of the Y axis to 1.50 m. Also, a comparison is made between the current model and the new model to observe the differences.

2. Methodology

Fig. 1 presents a circular footing with an eccentric column subjected to an axial load "P" and two moments "M_x and M_y" in orthogonal directions (biaxial bending).

The total resultant moment can be obtained as follows

$$M_{RT} = \sqrt{\left(M_x + Py_{fc}\right)^2 + \left(M_y + Px_{fc}\right)^2} \tag{1}$$

The inclination angle "α" with respect to the Y axis is obtained as follows

$$\alpha = arc\ tan\left(\frac{M_y + Px_{fc}}{M_x + Py_{fc}}\right) \tag{2}$$

Fig. 2 shows the resulting complete eccentricity diagram across the entire circular footing base.

The general biaxial bending equation is

$$\sigma = \frac{P}{A} + \frac{M_{xT}y}{I_x} + \frac{M_{yT}x}{I_y} \tag{3}$$

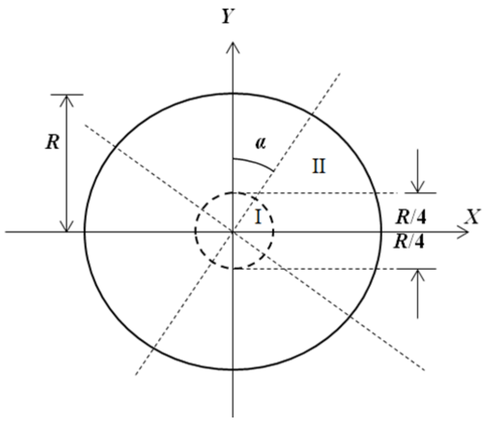

Fig. 2 Eccentricity diagram of a circular isolated footing

where: σ=pressure exerted by the ground on the base of the footing (kN/m^2), P=axial load (kN), A=ground contact area at the bottom of the footing (m^2), M_{xT}=total moment on the X axis (kN-m), M_{yT}=total moment on the Y axis (kN-m), I_x=moment of inertia on the X axis (m^4), I_y=moment of inertia on the Y axis (m^4), x=coordinate in the X direction of the base (m), y=coordinate in the Y direction of the base (m).

Substituting $A=\pi R^2$, $I=\pi R^4/4$ and Eq. (1) into Eq. (3), the maximum pressure "σ_a" and minimum pressure "σ_b" of the circular footing is obtained

$$\sigma_a = \frac{P}{\pi R^2} + \frac{4\sqrt{\left(M_x + Py_{fc}\right)^2 + \left(M_y + Px_{fc}\right)^2}}{\pi R^3} \tag{4}$$

$$\sigma_b = \frac{P}{\pi R^2} - \frac{4\sqrt{\left(M_x + Py_{fc}\right)^2 + \left(M_y + Px_{fc}\right)^2}}{\pi R^3} \tag{5}$$

where: R is the radius of the circular base.

2.1 Case I: Area works completely under compression

Fig. 3 presents a circular footing supported on elastic soils with an eccentric column under biaxial bending, assuming that the surface in contact with the ground works completely in compression and the distribution of the ground pressure is linear.

2.2 Case II: Area works partially under compression

Fig. 4 presents a circular footing supported on elastic soils with an eccentric column under biaxial bending, assuming that the surface in contact with the ground works partially in compression and the distribution of the ground pressure is linear.

The general equation of a plane in 3-D of the soil pressure on the footing is

$$A_1 x + A_2 y + A_3 \sigma_z + A_4 = 0 \tag{6}$$

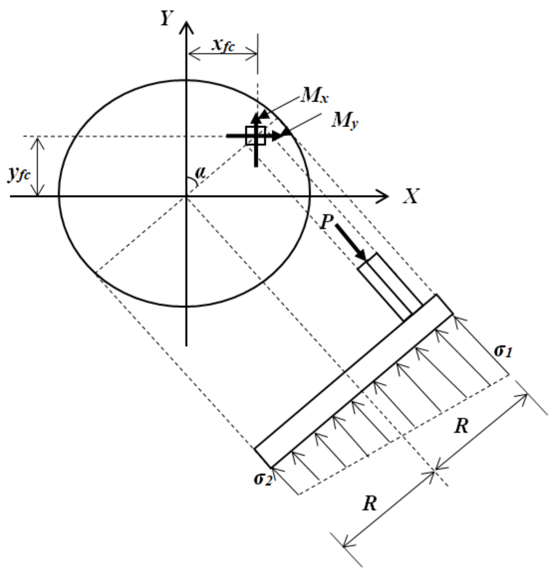

Fig. 3 Circular isolated footing works completely in compression

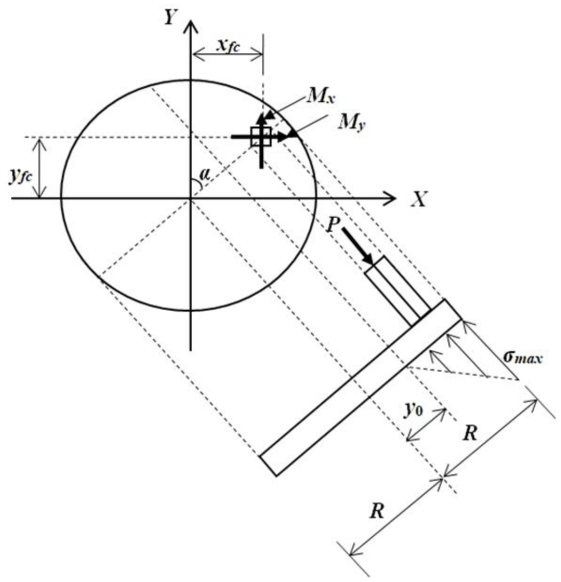

Fig. 4 Circular isolated footing works partially in compression

The three known points of the plane in 3D are (see Fig. 5)

$$P_1(R\sin\alpha\,, R\cos\alpha\,, \sigma_{\max}), P_2\left(y_0\sin\alpha - \sqrt{R^2 - {y_0}^2}\cos\alpha\,, y_0\cos\alpha + \sqrt{R^2 - {y_0}^2}\sin\alpha\,, 0\right), P_3\left(y_0\sin\alpha + \sqrt{R^2 - {y_0}^2}\cos\alpha\,, y_0\cos\alpha - \sqrt{R^2 - {y_0}^2}\sin\alpha\,, 0\right) \quad (7)$$

The coordinates of any point in the 3D plane are: $P_G\ (x, y, \sigma_z)$.
The general equation in the plane by determinant is obtained

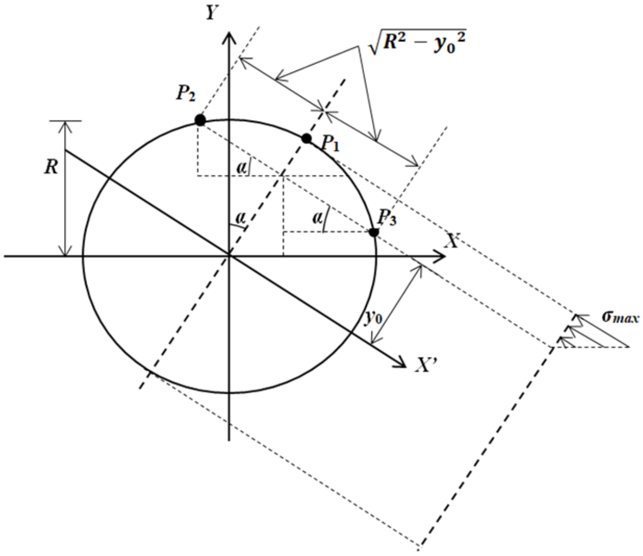

Fig. 5 Coordinates of the three known points of the plane in 3D

$$\begin{vmatrix} x - R\sin\alpha & y - R\cos\alpha & \sigma_z - \sigma_{\max} \\ y_0\sin\alpha - \sqrt{R^2 - y_0{}^2}\cos\alpha - R\sin\alpha & y_0\cos\alpha + \sqrt{R^2 - y_0{}^2}\sin\alpha - R\cos\alpha & 0 - \sigma_{\max} \\ y_0\sin\alpha + \sqrt{R^2 - y_0{}^2}\cos\alpha - R\sin\alpha & y_0\cos\alpha - \sqrt{R^2 - y_0{}^2}\sin\alpha - R\cos\alpha & 0 - \sigma_{\max} \end{vmatrix} \quad (8)$$

Solving the determinant and simplifying to obtain σ_z as a function of the coordinates (x, y), R, y_0 and α is obtained

$$\sigma_z = \frac{\sigma_{\max}(x\sin\alpha + y\cos\alpha - y_0)}{(R - y_0)} \quad (9)$$

The equation of the neutral axis (straight line), where the pressure is zero through Eq. (9) is obtained

$$x\sin\alpha + y\cos\alpha - y_0 = 0 \quad (10)$$

The general equations of the axial load "P", the two moments on the X and Y axes "M_x" and "M_y" are obtained as follows

$$P = \int_{-R}^{R}\int_{\frac{y_0 - x\sin\alpha}{\cos\alpha}}^{\sqrt{R^2-x^2}} \sigma_z\, dy\, dx \quad (11)$$

$$P = \frac{\sigma_{\max}R[2R^2(\cos\alpha)^2 - 3\pi|R|y_0\cos\alpha + 6y_0{}^2 + 2R^2]}{6(R - y_0)\cos\alpha} \quad (12)$$

$$M_x = \int_{-R}^{R}\int_{\frac{y_0 - x\sin\alpha}{\cos\alpha}}^{\sqrt{R^2-x^2}} \sigma_z\, y\, dy\, dx \quad (13)$$

Table 1 Circular isolated footing

Case	Constraint functions
I	Eqs. (4) and (5), $\sigma_a \leq \sigma_{max}$, $0 \leq \sigma_b$
II	Eqs. (1), (2), (12), (14), (16), $R \geq \lvert y_0 \rvert$

$$M_x = \frac{\sigma_{\max} R[8y_0R^2 - 24R^2y_0(\cos\alpha)^2 + 8{y_0}^3 + 3\pi|R|^3(\cos\alpha)^3]}{24(R - y_0)(\cos\alpha)^2} \tag{14}$$

$$M_y = \int_{-R}^{R}\int_{\frac{y_0 - x\sin\alpha}{\cos\alpha}}^{\sqrt{R^2-x^2}} \sigma_z y\,dy\,dx \tag{15}$$

$$M_y = \frac{\sigma_{max} R^3 \sin\alpha\,[3\pi|R|\cos\alpha - 16y_0]}{24(R - y_0)\cos\alpha} \tag{16}$$

where: $\sigma_{\max}$ is the available allowable bearing capacity of the soil.

2.3 Minimum area for circular isolated footings

The objective function to obtain the minimum area "$A_{\min}$" for both cases is

$$A_{\min} = \pi R^2 \tag{17}$$

Table 1 shows the constraint functions for the two cases.

Fig. 6 shows the flowchart using the Maple software to obtain the minimum area of a circular isolated footing in case II (Nonlinear optimization).

3. Numerical examples

Tables 2, 3 and 4 present the three cases to obtain the minimum area and the radius of the circular isolated footings subjected to biaxial bending due to the column.

Table 2 shows the results of the example 1 (x_{fc}=0 and y_{fc}=0) for three examples. Example 1.1: P_D=300 kN, P_L=200 kN, P=500 kN, M_{yD}=60 kN-m, M_{yL}=40 kN-m, M_y=100 kN-m, M_{xD}=180 kN-m, M_{xL}=120 kN-m, M_x=300 kN-m, M_R=316.23 kN-m, α=0.3217 Rad. Example 1.2: P_D=300 kN, P_L=200 kN, P=500 kN, M_{yD}=60 kN-m, M_{yL}=40 kN-m, M_y=100 kN-m, M_{xD}=120 kN-m, M_{xL}=80 kN-m, M_x=200 kN-m, M_R=223.61 kN-m, α=0.4636 Rad. Example 1.3: P_D=300 kN, P_L=200 kN, P=500 kN, M_{yD}=60 kN-m, M_{yL}=40 kN-m, M_y=100 kN-m, M_{xD}=90 kN-m, M_{xL}=60 kN-m, M_x=150 kN-m, M_R=180.28 kN-m, α=0.5880 Rad.

Table 3 presents the results of the example 2 (x_{fc}=1.50 m and y_{fc}=0) for three examples. Example 2.1: P_D=480 kN, P_L=320 kN, P=800 kN, M_{yD}=-480 kN-m, M_{yL}=-320 kN-m, M_y=-800 kN-m, M_{xD}=300 kN-m, M_{xL}=200 kN-m, M_x=500 kN-m, M_R=640.31 kN-m, α=0.6747 Rad. Example 2.2: P_D=480 kN, P_L=320 kN, P=800 kN, M_{yD}=-420 kN-m, M_{yL}=-280 kN-m, M_y=-700 kN-m, M_{xD}=300 kN-m, M_{xL}=200 kN-m, M_x=500 kN-m, M_R=707.11 kN-m, α=0.7854 Rad. Example 2.3: P_D=480 kN, P_L=320 kN, P=800 kN, M_{yD}=-360 kN-m, M_{yL}=-240 kN-m, M_y=-600 kN-m, M_{xD}=300 kN-m, M_{xL}=200 kN-m, M_x=500 kN-m, M_R=781.02 kN-m, α=0.8761 Rad.

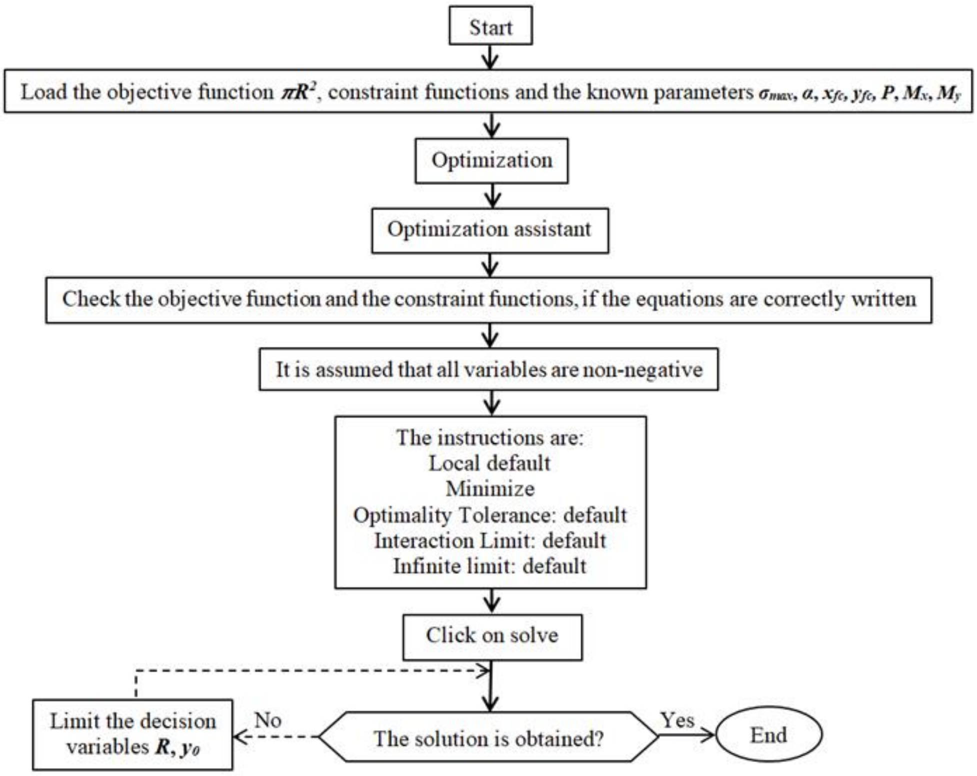

Fig. 6 Maple software flowchart for case II

Table 2 Example 1: x_{fc}=0 and y_{fc}=0

Example	σ_{max} (kN/m²)	Current Model	New Model		Proposed solution			σ_{maxpa} (kN/m²)	σ_{minpa} (kN/m²)
		R (m)	R (m)	y_0 (m)	R (m)	y_0 (m)	A_{min} (m²)		
1.1	250	2.53	1.41	-0.51	1.45	-0.58	6.61	227.89	0
	200	2.53	1.51	-0.68	1.55	-0.73	7.55	186.27	0
	150	2.53	1.67	-0.92	1.70	-0.97	9.08	142.58	0
	100	2.53	1.93	-1.34	1.95	-1.36	11.95	97.85	0
1.2	250	1.79	1.26	-0.76	1.30	-0.82	5.31	228.79	0
	200	1.79	1.37	-0.93	1.40	-0.98	6.16	187.17	0
	150	1.79	1.52	-1.17	1.55	-1.22	7.55	143.22	0
	100	1.79	1.79	-1.60	1.80	-1.62	10.18	97.97	0
1.3	250	1.44	1.18	-0.86	1.20	-0.89	4.52	241.68	0
	200	1.44	1.29	-1.03	1.30	-1.05	5.31	195.67	0
	150	1.45	1.44	-1.29	1.45	-1.30	6.61	147.66	0
	100	1.71	No solution		1.75	*	9.62	94.80	9.14

* The entire area of the footing is working in compression, where: σ_{maxpa} is the maximum pressure acting on the footing, σ_{minpa} is the minimum pressure acting on the footing.

Table 3 Example 2: x_{fc}=1.50 m and y_{fc}=0

Example	$\sigma_{\max}$ (kN/m^2)	Current Model	New Model		Proposed solution			σ_{maxpa} (kN/m^2)	σ_{minpa} (kN/m^2)
		R (m)	R (m)	y_0 (m)	R (m)	y_0 (m)	$A_{\min}$ (m^2)		
2.1	250	3.20	1.78	-0.59	1.80	-0.62	10.18	239.99	0
	200	3.20	1.91	-0.79	1.95	-0.85	11.95	187.16	0
	150	3.20	2.10	-1.08	2.15	-1.15	14.52	140.12	0
	100	3.20	2.42	-1.58	2.45	-1.62	18.86	96.80	0
2.2	250	3.54	1.84	-0.45	1.85	-0.46	10.75	246.98	0
	200	3.54	1.97	-0.64	2.00	-0.68	12.57	190.15	0
	150	3.54	2.15	-0.92	2.20	-0.99	15.21	140.68	0
	100	3.54	2.46	-1.41	2.50	-1.47	19.63	95.80	0
2.3	250	3.91	1.92	-0.26	1.95	-0.30	11.95	239.55	0
	200	3.91	2.04	-0.47	2.05	-0.48	13.20	197.67	0
	150	3.91	2.22	-0.76	2.25	-0.82	15.90	142.68	0
	100	3.91	2.51	-1.25	2.55	-1.29	20.43	99.55	0

Table 4 presents the results of the example 3 (x_{fc}=1.50 m and y_{fc}=1.50) for three examples. Example 3.1: P_D=480 kN, P_L=320 kN, P=800 kN, M_{yD}=-480 kN-m, M_{yL}=-320 kN-m, M_y=-800 kN-m, M_{xD}=300 kN-m, M_{xL}=200 kN-m, M_x=500 kN-m, M_R=1746.42 kN-m, α=0.2311 Rad. Example 3.2: P_D=480 kN, P_L=320 kN, P=800 kN, M_{yD}=-420 kN-m, M_{yL}=-280 kN-m, M_y=-700 kN-m, M_{xD}=300 kN-m, M_{xL}=200 kN-m, M_x=500 kN-m, M_R=1772.00 kN-m, α=0.2861 Rad. Example 3.3: P_D=480 kN, P_L=320 kN, P=800 kN, M_{yD}=-360 kN-m, M_{yL}=-240 kN-m, M_y=-600 kN-m, M_{xD}=300 kN-m, M_{xL}=200 kN-m, M_x=500 kN-m, M_R=1802.78 kN-m, α=0.3393 Rad.

4. Results

The proposed model can be verified as follows:

1. Substituting $x=R\sin\alpha$ and $y=R\cos\alpha$ into Eq. (9) is obtained $\sigma_z=\sigma_{\max}$.
2. Substituting $x=y_0\sin\alpha-\sqrt{R^2-{y_0}^2}\cos\alpha$ and $y=y_0\cos\alpha+\sqrt{R^2-{y_0}^2}\sin\alpha$ into Eq. (9) is obtained σ_z=0.
3. Substituting $x=y_0\sin\alpha+\sqrt{R^2-{y_0}^2}\cos\alpha$ and $y=y_0\cos\alpha-\sqrt{R^2-{y_0}^2}\sin\alpha$ into Eq. (9) is obtained σ_z=0.

Table 2 presents (Example 1: x_{fc}=0 and y_{fc}=0) the following: When σ_{max} decreases, the value of R is constant for the current model, and R and y_0 (absolute value) increase for the new model. This happens for the first two examples. For the third example, the value of R is constant for $\sigma_{\max}$=250 and 200 kN/m^2, and for $\sigma_{\max}$=150 and 100 kN/m^2 the value of R for the current model tends to decrease, and the new model shows the same behavior as the first two examples, but for $\sigma_{\max}$=100 kN/m^2 there is no solution.

Table 3 presents (Example 2: x_{fc}=1.50 m and y_{fc}=0) the following: When $\sigma_{\max}$ decreases, the value of R is constant for the current model, and R and y_0 (absolute value) increase for the new model. This happens for the three examples.

Table 4 Example 3: x_{fc}=1.50 m and y_{fc}=1.50 m

Example	σ_{max} (kN/m^2)	Current Model	New Model		Proposed solution			σ_{maxpa} (kN/m^2)	σ_{minpa} (kN/m^2)
		R (m)	R (m)	y_0 (m)	R (m)	y_0 (m)	A_{min} (m^2)		
3.1	250	8.73	3.01	1.14	3.05	1.06	29.22	229.27	0
	200	8.73	3.11	0.93	3.15	0.87	31.17	187.68	0
	150	8.73	3.29	0.65	3.30	0.63	34.21	146.63	0
	100	8.73	3.59	0.18	3.60	0.16	40.72	98.58	0
3.2	250	8.86	3.06	1.24	3.10	1.14	30.19	227.72	0
	200	8.86	3.16	1.00	3.20	0.91	32.17	183.44	0
	150	8.86	3.32	0.70	3.35	0.65	35.26	142.73	0
	100	8.86	3.62	0.22	3.65	0.17	41.85	96.14	0
3.3	250	9.01	3.15	1.40	3.20	1.13	32.17	206.23	0
	200	9.01	3.21	1.10	3.25	1.00	33.18	183.44	0
	150	9.01	3.36	0.77	3.40	0.69	36.32	140.69	0
	100	9.01	3.65	0.28	3.70	0.20	43.01	94.48	0

Table 4 presents (Example 3: x_{fc}=1.50 m and y_{fc}=1.50 m) the following: When σ_{max} decreases, the value of R is constant for the current model, and R increase and y_0 (absolute value) decreases for the new model. This happens for the three examples.

Fig. 7 shows the comparison between the current model and the new model for R of example 1, Fig. 8 presents the comparison between the current model and the new model for R of example 2, and Fig. 9 shows the comparison between the current model and the new model for R of example 3.

Fig. 7 shows the following results (Example 1): The smaller radius appears in the new model with respect to the current model in all examples, except in example 1.3 at σ_{max}=150 kN/m^2 it is equal and at σ_{max}=100 kN/m^2 the current model is smaller because the new model has no solution. The largest difference is 1.79 times the current model than the new model in example 1.1 in σ_{max}=250 kN/m^2.

Fig. 8 shows the following results (Example 2): The smaller radius appears in the new model with respect to the current model in all examples. The largest difference is 2.04 times the current model than the new model in example 2.3 in σ_{max}=250 kN/m^2.

Fig. 9 shows the following results (Example 3): The smaller radius appears in the new model with respect to the current model in all examples. The largest difference is 2.90 times the current model than the new model in example 3.1 in σ_{max}=250 kN/m^2.

5. Conclusions

This study aims is present a new model to obtain the minimum area in circular isolated footings with eccentric column taking into account that the surface in contact with the ground works partially in compression, i.e., a part of the contact area of the footing is subject to compression and the other there is no pressure (pressure zero).

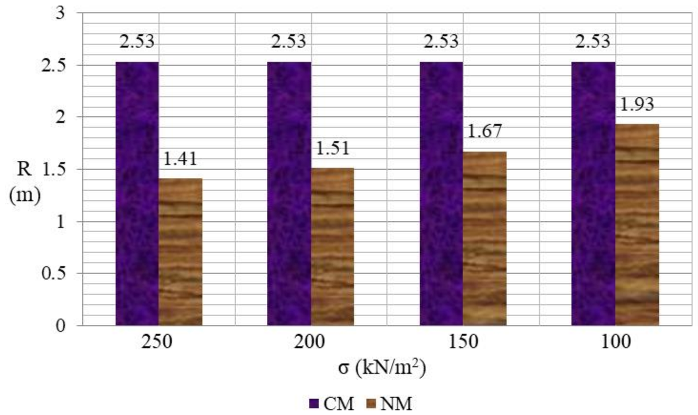

Example 1.1

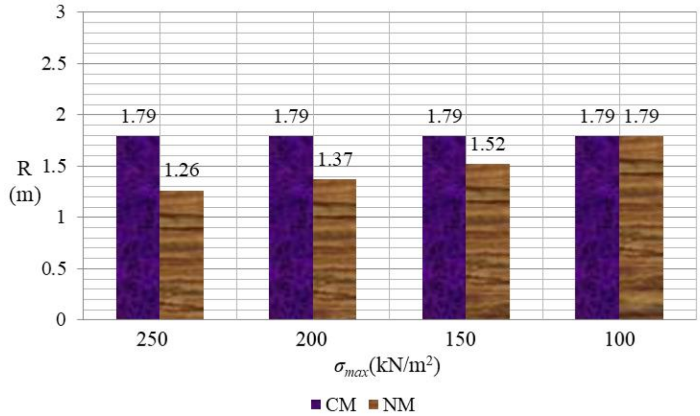

Example 1.2

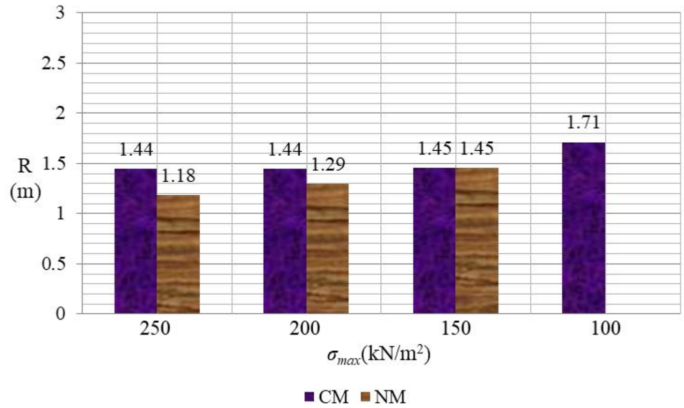

Example 1.3

Fig. 7 Example 1

This research shows the minimum area for circular isolated footings under biaxial bending. Assuming that the footing is rigid, the column is eccentrically placed, supported on elastic soils, and the pressure diagram is linear.

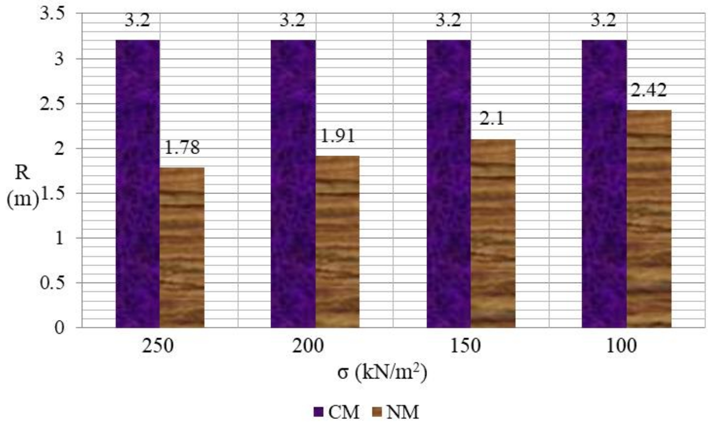

Example 2.1

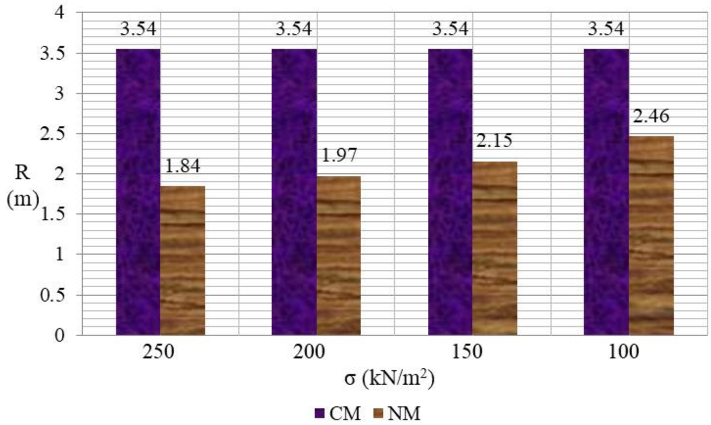

Example 2.2

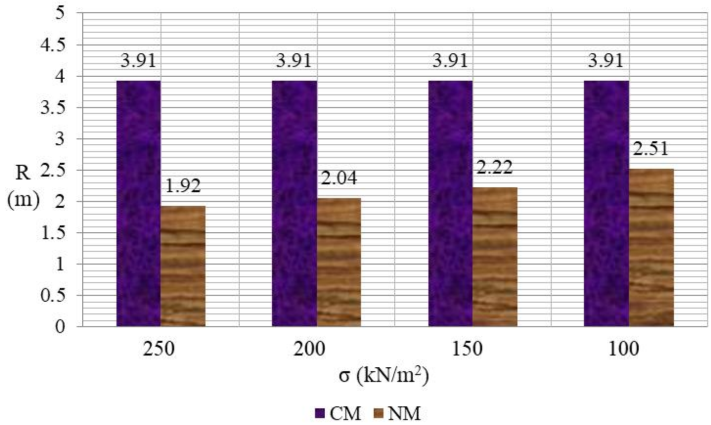

Example 2.3

Fig. 8 Example 2

The current model is presented as follows: the independent variables (known data) are σ_{max}, x_{fc}, y_{fc}, P, M_x and M_y, and the dependent variables are A_{min}, R, σ_1 and σ_2 (data to obtain).

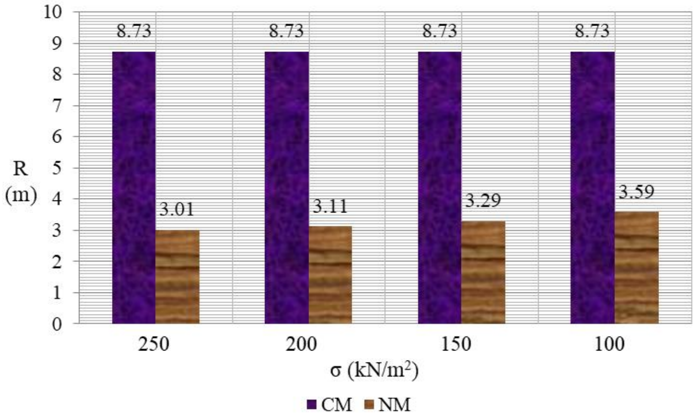

Example 3.1

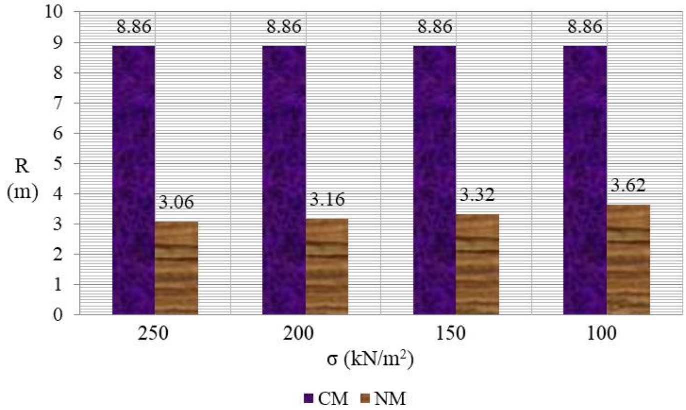

Example 3.2

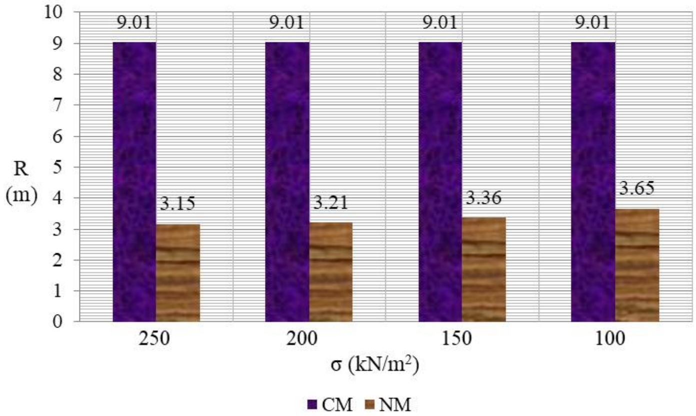

Example 3.3

Fig. 9 Example 3

The new model is developed as follows: the independent variables (known data) are $\sigma_{\max}$, x_{fc}, y_{fc}, P, M_x and M_y, and the dependent variables are $A_{\min}$, R, y_0 and α (data to obtain).

The contributions of this paper are:

1) The normal practice in structural engineering is to use the trial and error procedure to obtain the radius and area of the circular footing.

2) Other engineers determine the radius and area of circular footing under biaxial bending supported on elastic soils, but considering a non-eccentric column.

3) This methodology can be used to verify of the allowable load capacity of the soil, considering the objective function "σ_{max}", and the same constraint functions.

4) The new model shows a great saving compared to the current model of 44.27% in Example 1 (see Fig. 7), 50.90% in Example 2(see Fig. 8) and 65.04% in Example 3 (see Fig. 9).

Suggestions for future research may be:

1.- Minimum cost design for circular isolated footings with eccentric column taking into account that the surface in contact with the ground works partially in compression.

2.- Minimum area for rectangular isolated footings with eccentric column taking into account that the surface in contact with the ground works partially in compression.

3.- Minimum cost design for rectangular isolated footings with eccentric column taking into account that the surface in contact with the ground works partially in compression.

Acknowledgments

The research described in this paper was financially supported by the Universidad Autónoma de Coahuila and Universidad Juárez del Estado de Durango, Mexico.

References

Agrawal, R. and Hora, M.S. (2012), "Nonlinear interaction behaviour of infilled frame-isolated footings-soil system subjected to seismic loading", *Struct. Eng. Mech.*, **44**(1), 85-107. https://doi.org/10.12989/sem.2012.44.1.085.

Aguilera-Mancilla, G., Luévanos-Rojas, A., López-Chavarría, S. and Medina-Elizondo, M. (2019), "Modeling for the strap combined footings Part I: Optimal dimensioning", *Steel Compos. Struct.*, **30**(2), 97-108. https://doi.org/10.12989/scs.2019.30.2.097.

Al-Ansari, M.S. (2013), "Structural cost of optimized reinforced concrete isolated footing", *Int. Scholar. Scientif. Res. Innov.*, **7**(4), 193-200.

Al-Ansari, M.S. (2014), "Cost of reinforced concrete paraboloid shell footing", *J. Struct. Anal. Des.*, **1**(3), 111-119.

Alazwari, M.A., Daikh, A.A., Houari, M.S.A., Tounsi, A. and Eltaher, M.A. (2021), "On static buckling of multilayered carbon nanotubes reinforced composite nanobeams supported on non-linear elastic foundations", *Steel Compos. Struct.*, **40**(3), 389-404. https://doi.org/10.12989/scs.2021.40.3.389.

Alijani, M. and Bidgoli, M.R. (2018), "Agglomerated SiO2 nanoparticles reinforced-concrete foundations based on higher order shear deformation theory: Vibration analysis", *Adv. Concrete Constr.*, **6**(6), 585-610. https://doi.org/10.12989/acc.2018.6.6.585.

Anil, Ö., Akbaş, S.O., BabagĪray, S., Gel, A.C. and Durucan, C. (2017), "Experimental and finite element analyses of footings of varying shapes on sand", *Geomech. Eng.*, **12**(2), 223-238. https://doi.org/10.12989/gae.2017.12.2.223.

Basudhar, P.K., Dey, A. and Mondal, A.S. (2012), "Optimal Cost-Analysis and Design of Circular Footings", *Int. J. Eng. Technol. Innov.*, **2**(4), 243-264.

Dagdeviren, U. (2016), "Shear stresses below the rectangular foundations subjected to biaxial bending", *Geomech. Eng.*, **10**(2), 189-205. https://doi.org/10.12989/gae.2016.10.2.189.

Garay-Gallegos, J.R., Luévanos-Rojas, A., López-Chavarría, S., Medina-Elizondo, M., Aguilera-Mancilla, G. and García-Canales, E. (2022), "A comparative study between the new model and the current model for T-shaped combined footings", *Geomech. Eng.*, **30**(6), 525-538. https://doi.org/10.12989/gae.2022.30.6.525.

García-Galván, M., Luévanos-Rojas, A., López-Chavarría, S., Medina-Elizondo, M. and Rivera-Mendoza, J.B. (2022), "A general model for rectangular footings Part I: Optimal surface", *DYNA: Revista de la Facultad de Minas. Universidad Nacional de Colombia. Sede Medellín*, **89**(221), 132-141. https://doi.org/10.15446/dyna.v89n221.100028.

García-Galván, M., Luévanos-Rojas, A., López-Chavarría, S., Medina-Elizondo, M. and Rivera-Mendoza, J.B. (2022), "A comparative study between trapezoidal combined footings and T-shaped combined footings", *Couple. Syst. Mech.*, **11**(3), 233-257. https://doi.org/10.12989/csm.2022.11.3.233.

García-Graciano, M.L., Luévanos-Rojas, A., López-Chavarría, S. and Medina-Elizondo, M. (2022), "Mathematical modeling for corner strap combined footings resting on the ground: Part 1", *Computación y Sistemas*, **26**(4), 1429-1443. http://dx.doi.org/10.13053/cys-26-4-4080.

Golewski, G.L. (2019), "New principles for implementation and operation of foundations for machines: A review of recent advances", *Struct. Eng. Mech.*, **71**(3), 317-327. https://doi.org/10.12989/sem.2019.71.3.317.

Gör, M. (2022), "Analyzing the bearing capacity of shallow foundations on two-layered soil using two novel cosmology-based optimization techniques", *Smart Struct. Syst.*, **29**(3), 513-522. https://doi.org/10.12989/sss.2022.29.3.513.

Hadzalic, E., Ibrahimbegovic, A. and Dolarevic, S. (2018), "Failure mechanisms in coupled soil-foundation systems", *Couple. Syst. Mech.*, **7**(1), 27-42. https://doi.org/10.12989/csm.2018.7.1.027.

Hadzalic, E., Ibrahimbegovic, A. and Dolarevic, S. (2018), "Failure mechanisms in coupled poro-plastic medium", *Couple. Syst. Mech.*, **7**(1), 43-59. https://doi.org/10.12989/csm.2018.7.1.043.

Hadzalic, E., Ibrahimbegovic, A. and Dolarevic, S. (2018), "Fluid-structure interaction system predicting both internal pore pressure and outside hydrodynamic pressure", *Couple. Syst. Mech.*, **7**(6), 649-668. https://doi.org/10.12989/csm.2018.7.6.649.

Hadzalic, E., Ibrahimbegovic, A. and Dolarevic, S. (2020), "3D thermo-hydro-mechanical coupled discrete beam lattice model of saturated poro-plastic medium", *Couple. Syst. Mech.*, **9**(2), 125-145. https://doi.org/10.12989/csm.2020.9.2.125.

Himeur, N., Mamen, B., Benguediab, S., Bouhadra, A., Menasria, A., Bouchouicha, B., Bourada, F., Benguediab, M. and Tounsi, A. (2022), "Coupled effect of variable Winkler–Pasternak foundations on bending behavior of FG plates exposed to several types of loading", *Steel Compos. Struct.*, **44**(3), 353-369. https://doi.org/10.12989/scs.2022.44.3.353.

Ibrahimbegovic, A. and Mejia-Nava, R.A. (2021), "Heterogeneities and material-scales providing physically based damping to replace Rayleigh damping for any structure size", *Couple. Syst. Mech.*, **10**(3), 201-216. https://doi.org/10.12989/csm.2021.10.3.201.

Jelusic, P. and Zlender, B. (2018), "Optimal design of pad footing based on MINLP optimization", *Soil. Found.*, **58**(2), 277-289. https://doi.org/10.1016/j.sandf.2018.02.002.

Kaur, A. and Kumar, A. (2016), "Behavior of eccentrically inclined loaded footing resting on fiber reinforced soil", *Geomech. Eng.*, **10**(2), 155-174. https://doi.org/10.12989/gae.2016.10.2.155.

Khajehzadeh, M., Taha M.R. and Eslami, M. (2014), "Multi-objective optimization of foundation using global-local gravitational search algorithm", *Struct. Eng. Mech.*, **50**(3), 257-273. http://doi.org/10.12989/sem.2014.50.3.257.

Kim-Sánchez, D.S., Luévanos-Rojas, A., Barquero-Cabrero, J.D., López-Chavarría, S., Medina-Elizondo, M. and Luévanos-Soto, I. (2022), "A new model for the complete design of circular isolated footings considering that the contact surface works partially under compression", *Int. J. Innov. Comput. I.*, **18**(6), 1769-1784.

Lee, J., Jeong, S. and Lee, J.K. (2015), "3D analytical method for mat foundations considering coupled soil springs", *Geomech. Eng.*, **8**(6), 845-850. https://doi.org/10.12989/gae.2015.8.6.845.

Lezgy-Nazargah, M., Mamazizi, A. and Khosravi, H. (2022), "Analysis of shallow footings rested on tensionless foundations using a mixed finite element model", *Struct. Eng. Mech.*, **81**(3), 379-394. https://doi.org/10.12989/sem.2022.81.3.379.

López-Chavarría, S., Luévanos-Rojas, A. and Medina-Elizondo, M. (2017a), "Optimal dimensioning for the corner combined footings", *Adv. Comput. Des.*, **2**(2), 169-183. https://doi.org/10.12989/acd.2017.2.2.169.

López-Chavarría, S., Luévanos-Rojas, A. and Medina-Elizondo, M. (2017b), "A mathematical model for dimensioning of square isolated footings using optimization techniques: General case", *Int. J. Innov. Comput. I.*, **13**(1), 67-74.

López-Chavarría, S., Luévanos-Rojas, A., Medina-Elizondo, M., Sandoval-Rivas, R. and Velázquez-Santillán, F. (2019), "Optimal design for the reinforced concrete circular isolated footings", *Adv. Comput. Des.*, **4**(3), 273-294. https://doi.org/10.12989/acd.2019.4.3.273.

Luat, N.V., Lee, K. and Thai, D.K. (2020), "Application of artificial neural networks in settlement prediction of shallow foundations on sandy soils", *Geomech. Eng.*, **20**(5), 385-397. https://doi.org/10.12989/gae.2020.20.5.385.

Luévanos-Rojas, A. (2014a), "A comparative study for dimensioning of footings with respect to the contact surface on soil", *Int. J. Innov. Comput. I.*, **10**(4), 1313-1326.

Luévanos-Rojas, A. (2014b), "Design of isolated footings of circular form using a new model", *Struct. Eng. Mech.*, **52**(4), 767-786. https://doi.org/10.12989/sem.2014.52.4.767.

Luévanos-Rojas, A. (2015a), "A new mathematical model for dimensioning of the boundary trapezoidal combined footings", *Int. J. Innov. Comput. I.*, **11**(4), 1269-1279.

Luévanos-Rojas, A. (2015b), "Design of boundary combined footings of trapezoidal form using a new model", *Struct. Eng. Mech.*, **56**(5), 745-765. http://doi.org/10.12989/sem.2015.56.5.745.

Luévanos-Rojas, A. (2016a), "A comparative study for the design of rectangular and circular isolated footings using new models", *Dyna*, **83**(196), 149-158. https://doi.org/10.15446/dyna.v83n196.51056.

Luévanos-Rojas, A. (2016b), "A mathematical model for the dimensioning of combined footings of rectangular shape", *Revista Técnica de la Facultad de Ingeniería Universidad del Zulia*, **39**(1), 3-9.

Luévanos-Rojas, A. (2023a), "Minimum cost design for rectangular isolated footings taking into account that the column is located in any part of the footing", *Build.*, **13**(9), 1-16. https://doi.org/10.3390/buildings13092269.

Luévanos-Rojas, A. (2023b), "Optimization for trapezoidal combined footings: Optimal design", *Adv. Concrete Constr.*, **16**(1), 21-34. https://doi.org/10.12989/acc.2023.16.1.021.

Luévanos-Rojas, A. (2023c), "New model for complete design of rectangular isolated footings taking into account that the contact surface works partially in compression", *Revista ALCONPAT*, **13**(2), 192-219. https://doi.org/10.21041/ra.v13i2.671.

Luévanos-Rojas, A., Barquero-Cabrero, J.D., López-Chavarría, S. and Medina-Elizondo, M. (2017b), "A comparative study for design of boundary combined footings of trapezoidal and rectangular forms using new models", *Couple. Syst. Mech.*, **6**(4), 417-437. https://doi.org/10.12989/csm.2017.6.4.417.

Luévanos-Rojas, A., López-Chavarría, S. and Medina-Elizondo, M. (2017a), "Optimal design for rectangular isolated footings using the real soil pressure", *Ingeniería e Investigación*, **37**(2), 25-33. https://doi.org/10.15446/ing.investig.v37n2.61447.

Luévanos-Rojas, A., López-Chavarría, S. and Medina-Elizondo, M. (2018a), "A new model for T-shaped combined footings Part I: Optimal dimensioning", *Geomech. Eng.*, **14**(1), 51-60. https://doi.org/10.12989/gae.2018.14.1.051.

Luévanos-Rojas, A., López-Chavarría, S. and Medina-Elizondo, M. (2018b), "A new model for T-shaped combined footings Part II: Mathematical model for design", *Geomech. Eng.*, **14**(1), 61-69. https://doi.org/10.12989/gae.2018.14.1.061.

Luévanos-Rojas, A., López-Chavarría, S., Medina-Elizondo, M., Sandoval-Rivas, R. and Farías-Montemayor, O.M. (2020), "An analytical model for the design of corner combined footings", *Revista ALCONPAT*, **10**(3), 317-335. https://doi.org/10.21041/ra.v10i3.432.

Malapur, M.M., Cholappanavar, P. and Fernandes, R.J. (2018), "Optimization of RC column and footings using genetic algorithm", *Int. Res. J. Eng. Technol. (IRJET)*, **5**(8), 546-552.

Mohebkhah, A. (2017), "Bearing capacity of stripfootingson a stone masonry trench in clay", *Geomech.*

Eng., **13**(2), 255-267. https://doi.org/10.12989/gae.2017.13.2.255.

Montes-Paramo, P., Luévanos-Rojas, A., López-Chavarría, S., Medina-Elizondo, M. and Sandoval-Rivas, R. (2023), "Optimal area for rectangular combined footings assuming that the contact surface with the soil works partially to compression", *Ingeniería Investigación y Tecnología*, **24**(02), 1-15. https://doi.org/10.22201/fi.25940732e.2023.24.2.012.

Moreno-Hernández, M.A., Luévanos-Rojas, A., López-Chavarría, S. and Medina-Elizondo, M. (2022), "Mathematical modeling for corner strap combined footings resting on the ground: Part 1", *Computación y Sistemas*, **26**(3), 1259-1272. http://doi.org/10.13053/cys-26-3-4079.

Pasillas-Orona, A.I., Luévanos-Rojas, A., López-Chavarría, S., Medina-Elizondo, M. and Aguilera-Mancilla, G. (2020), "Un modelo optimizado para zapatas combinadas trapezoidales apoyadas sobre el terreno: Superficie óptima", *Acta Universitaria*, **30**, 1-18. http://doi.org/10.15174/au.2020.2973.

Rad, A.B. (2012), "Static response of 2-D functionally graded circular plate with gradient thickness and elastic foundations to compound loads", *Struct. Eng. Mech.*, **44**(2), 139-161. https://doi.org/10.12989/sem.2012.44.2.139.

Ramu, K. and Madhav, M.R. (2010), "Response of rigid footing on reinforced granular fill over soft soil", *Geomech. Eng.*, **2**(4), 281-302. https://doi.org/10.12989/gae.2010.2.4.281.

Rawat, S. and Mittal, R.K. (2018), "Optimization of eccentrically loaded reinforced-concrete isolated footings", *Pract. Period. Struct. Des. Constr.*, **23**(2), 06018002. https://doi.org/10.1061/(ASCE)SC.1943-5576.0000366.

Rivera-Mendoza, J.B., Luévanos-Rojas, A., López-Chavarría, S., Medina-Elizondo, M. and García-Galván, M. (2022), "general model for rectangular footings Part II: Modeling for design", *Dyna*, **89**(223), 9-18. https://doi.org/10.15446/dyna.v89n223.100030.

Rizwan, M., Alam, B., Rehman, F.U., Masud, N., Shahzada, K. and Masud, T. (2012), "Cost optimization of combined footings using modified complex method of box", *Int. J. Adv. Struct. Geotech. Eng.*, **1**(1), 24-28.

Soto-García, S., Luévanos-Rojas, A., Barquero-Cabrero, J.D., López-Chavarría, S., Medina-Elizondo, M., Farias-Montemayor, O.M. and Martinez-Aguilar, C. (2022), "A new model for the contact surface with soil of circular isolated footings considering that the contact surface works partially under compression", *Int. J. Innov. Comput. I.*, **18**(4), 1103-1116.

Turedi, Y., Emirler, B., Ornek, M. and Yildiz, A. (2019), "Determination of the bearing capacity of model ring footings: Experimental and numerical investigations", *Geomech. Eng.*, **18**(1), 29-39. https://doi.org/10.12989/gae.2019.18.1.029.

Vela-Moreno, V.B., Luévanos-Rojas, A., López-Chavarría, S., Medina-Elizondo, M., Sandoval-Rivas, R. and Martinez-Aguilar, C. (2022), "Optimal area for rectangular isolated footings considering that contact surface works partially to compression", *Struct. Eng. Mech.*, **84**(4), 561-573. https://doi.org/10.12989/sem.2022.84.4.561.

Velázquez-Santillán, F., Luévanos-Rojas, A., López-Chavarría, S., Medina-Elizondo, M. and Sandoval-Rivas, R. (2018), "Numerical experimentation for the optimal design for reinforced concrete rectangular combined footings", *Adv. Comput. Des.*, **3**(1), 49-69. https://doi.org/10.12989/acd.2018.3.1.049.

Yáñez-Palafox, J.A., Luévanos-Rojas, A., López-Chavarría, S. and Medina-Elizondo, M. (2019), "Modeling for the strap combined footings Part II: Mathematical model for design", *Steel Compos. Struct.*, **30**(2), 109-121. https://doi.org/10.12989/scs.2019.30.2.109.

AI